Article:

Réjou-Méchain, M, Tymen, B, Blanc, L et al. (6 more authors) (2015) Using repeated small-footprint LiDAR acquisitions to infer spatial and temporal variations of a high-biomass Neotropical forest. Remote Sensing of Environment, 169. 93 - 101. ISSN 0034-4257

https://doi.org/10.1016/j.rse.2015.08.001

Title: Using repeated small-footprint LiDAR acquisitions to infer spatial and temporal variations of a high-biomass Neotropical forest.

Authors: Maxime Réjou-Méchain[a,b*], Blaise Tymen[a], Lilian Blanc[c], Sophie Fauset[d], Ted R. Feldpausch[d,e], Abel Monteagudo[f], Oliver L. Phillips[d], Hélène Richard[g], Jérôme Chave[a]

Authors affiliation:

[a]Laboratoire Evolution et Diversité Biologique, UMR 5174 CNRS, Université Paul Sabatier, 31062 Toulouse, France.

[b]French Institute of Pondicherry, UMIFRE 21/USR 3330 CNRS-MAEE, Pondicherry, India.

[c] CIRAD-ES, UR "Biens et Services des Ecosystèmes forestiers", Embrapa-Belém, Brazil

[d] School of Geography, University of Leeds, Leeds, UK

[e] Geography, College of Life and Environmental Sciences, University of Exeter, Rennes Drive, Exeter, UK

[f]Jardín Botánico de Missouri, Oxapampa, Peru.

[g]Office National des Forêts Guyane, service développement Sylvétude, Réserve Montabo, 97307 Cayenne, French Guiana

***Corresponding author:** Maxime Réjou-Méchain; Phone: 0033 5 61 55 85 81; Fax: 0033 5 61 55 73 27 ; E-mail: maxime.rejou@gmail.com

Abstract

In recent years, LiDAR technology has provided accurate forest aboveground biomass (AGB) maps in several forest ecosystems, including tropical forests. However, its ability to accurately map forest AGB changes in high-biomass tropical forests has seldom been investigated. Here, we assess the ability of repeated LiDAR acquisitions to map AGB stocks and changes in an old-growth Neotropical forest of French Guiana. Using two similar aerial small-footprint LiDAR campaigns over a four year interval, spanning ca. 20 km^2, and concomitant ground sampling, we constructed a model relating median canopy height and AGB at a 0.25-ha and 1-ha resolution. This model had an error of 14% at a 1-ha resolution (RSE=54.7 Mg ha^{-1}) and of 23% at a 0.25-ha resolution (RSE=86.5 Mg ha^{-1}). This uncertainty is comparable with values previously reported in other tropical forests and confirms that aerial LiDAR is an efficient technology for AGB mapping in high-biomass tropical forests. Our map predicts a mean AGB of 340 Mg ha^{-1} within the landscape. We also created an AGB change map, and compared it with ground-based AGB change estimates. The correlation was weak but significant only at the 0.25-ha resolution. One interpretation is that large natural tree-fall gaps that drive AGB changes in a naturally regenerating forest can be picked up at fine spatial scale but are veiled at coarser spatial resolution. Overall, both field-based and LiDAR-based estimates did not reveal a detectable increase in AGB stock over the study period, a trend observed in almost all forest types. Small footprint LiDAR is a powerful tool to dissect the fine-scale variability of AGB and to detect the main ecological controls underpinning forest biomass variability both in space and time.

Keywords: LiDAR; Aboveground biomass; Forest carbon; Tropical forest; Forest dynamic.

1. Introduction

Tropical forests play an important role in the terrestrial carbon cycle. Tropical deforestation and degradation are a large source of carbon (C) emissions into the atmosphere, contributing some 7-15% to the total anthropogenic C emissions since the early 2000s (Pan et al. 2011; Harris et al. 2012). This carbon loss from the terrestrial biosphere is thought to be approximately balanced by forest regrowth and by an increase in terrestrial ecosystem carbon storage ability through time related to global or regional forcings, such as CO_2 fertilization, temperature increase, or rainfall fluctuations (Lewis *et al.* 2009; Pan *et al.* 2011). An effective strategy for mitigating anthropogenic CO_2 emissions is to implement national and international governance agreements that will help curb deforestation and forest degradation (Agrawal et al. 2011). To meet this challenge, it is essential to implement robust techniques for the quantification of carbon stocks and changes in tropical forests (Chave et al. 2005; Saatchi et al. 2011; Le Toan et al. 2011; Clark & Kellner 2012).

Light detection and ranging sensors (LiDAR), a technology dating back to the early 1980s (Arp & Tranarg 1982; Aldred & Bonner 1985), has now made impressive progress and is being routinely used to determine forest structural characteristics (Lefsky *et al.* 2002). The high spatial resolution of current airborne LiDAR systems and their ability to cover large remote areas make it an attractive option for conservation and/or management programs and for the implementation of landscape-scale GHG emission mitigation strategies (Agrawal et al. 2011). In mixed-species, closed-canopy tropical forests, studies using a LiDAR system to infer forest structural parameters date back at least to the early 2000s (Drake *et al.* 2002, 2003), and they have since been applied broadly in the Neotropics (e.g. d'Oliveira *et al.* 2012; Vincent *et al.* 2012; Asner *et al.* 2013a; b), in South-East Asia (Englhart *et al.* 2013; Jubanski *et al.* 2013) and in Africa (Asner *et al.* 2012a; b; Vaglio Laurin *et al.* 2014). Zolkos *et al*. (2013) have conducted a meta-analysis including over 70 studies that used LiDAR for forest aboveground biomass (AGB) retrieval. Of these, 10 studies were conducted in forests with a mean AGB > 300 Mg ha^{-1}, and only one of these studies was in the tropics (Hawaii; Asner *et al.* 2009). In light of the fast pace of publications on this research theme, two challenges appear to be outstanding.

First, it is important to document the errors associated with LiDAR-AGB models in the high-biomass forested areas of the tropics, notably because the absolute errors associated with LiDAR-AGB models are expected to be significantly higher in such high-biomass areas (Zolkos *et al.* 2013). Second, the direct monitoring of changes in AGB in tropical forests is a crucial challenge in carbon accounting programs, and it appears to be now possible from remotely sensed instruments at least in areas undergoing deforestation and degradation (Asner *et al.* 2005). However, the ability of this technique to describe the natural dynamics of old-growth forests is still outstanding. Encouraging results have been obtained in temperate and in boreal forests (Hudak *et al.* 2012; Bollandsås *et al.* 2013; Næsset *et al.* 2013; Skowronski *et al.* 2014). However, tests in tropical forests have thus far been less conclusive. To our knowledge, only two published studies have sought to compare the performance of LiDAR and ground-based data to measure the AGB dynamics of tropical forests. The first study was conducted at La Selva, Costa Rica, and used large-footprint airborne LiDAR data (Dubayah *et al.* 2010). The second study was conducted at Barro Colorado Island, Panama, and used a combination of small- and large-footprint LiDAR (Meyer *et al.* 2013). Both studies found a weak relationship between changes in LiDAR metrics and field-measured AGB changes. One possible interpretation is that the signature of natural forest dynamics is too subtle to be detectable by change in LiDAR metrics (Dubayah *et al.* 2010). However, the use of large footprint sensors or systematic differences in accuracy across LiDAR sensors may also explain these results (Zolkos *et al.* 2013).

Forests of the Guiana Shield hold the highest AGB values and the tallest forests of the Neotropics (Feldpausch *et al.* 2011, 2012; Saatchi *et al.* 2011). Their AGB stock is comparable to that reported in central Africa and in some forests of South-East Asia (Slik *et al.* 2013). Using two LiDAR campaigns conducted at four-year intervals combined with intensive and concomitant ground sampling (15,438 trees monitored over almost 30 ha), we infer the spatial and temporal variation of AGB in an old growth tropical forest landscape of French Guiana (Fig. 1). We specifically ask the two following questions: i) Can the spatial variation in AGB be detected accurately using LiDAR in tall, high-biomass, tropical forests?; ii) How do LiDAR-derived temporal changes in AGB compare with field-derived estimates?

2. Materials and methods

2.1. Study area

Our study was carried out in the lowland rain forest of French Guiana at the Nouragues Ecological Research Station (Fig. 1 and 2). The landscape corresponds to a succession of hills, ranging between 26-280 m asl, with a granitic outcrop (inselberg) reaching 430 m asl. Rainfall is 2861 mm y^{-1} (average 1992-2012), with a 2-mo dry season (< 100 mm $month^{-1}$) during September and October, and a shorter dry season in March. Human activity is unlikely to have induced major disturbances in recent history: now extinct Nouragues Amerindians are reported to have inhabited this area during the eighteenth century, but departed further south some 200 years ago. The forest around the station harbours a diverse flora (Sabatier & Prévost 1990; van der Meer & Bongers 1996), with over 1700 angiosperm species recorded in the Natural Reserve.

2.2. LiDAR data acquisition

Two acquisitions of small footprint discrete return LiDAR were conducted in the Nouragues research area. The first coverage was conducted in two steps, in November 2007 and November 2008 for a total area of 1,900 ha (Fig. S1a). This first acquisition was based on a portable Riegl laser rangefinder (LMS6Q140i-60) positioned on a helicopter flying at about 30 m s^{-1} ca 150 m above the ground. This rangefinder system is a time-of-flight measurement of 30 kHz laser pulse in the infrared wavelength region (0.9 μm) with a footprint of 0.45 m and a scan angle of 60°. The average laser point density was ca. 4 imp/m^2 and acquisitions were all conducted in last return mode to maximise penetration (the system used did not have multiple return registering capacity). The second acquisition occurred in March 2012 and covered an area of 2,400 ha (Fig. S1b). Acquisition was based on a portable Riegl laser rangefinder (LMS-Q560) embarked on a Falcon aircraft at a speed ca 45 m s^{-1} about 400 m above the ground. It used a 200 kHz laser pulse in the infrared wavelength region (1.5 μm) with a footprint of 0.25 m and a scan angle of 45°. The average laser point density was ca. 20 imp/m^2 (the system had multiple returns registering capacity). This pulse density is much higher than most previous studies, ensuring a good canopy penetration rate and thus an accurate digital elevation model. In both acquisitions, the systems included two dual-frequency GPS receivers coupled to an inertial navigation system, ensuring that a sub-decimeter differential position can be calculated at the post-processing stage. The area of overlap of the two acquisitions was ca. 1,400 ha. The two LiDAR campaigns were contracted by a private company (http://www.altoa.fr/).

2.3. LiDAR data processing

A major challenge, especially in dense tropical forests, is to identify the LiDAR echoes that lie on the probable ground surface (i.e. bare-earth points). The number of bare-earth points directly affects the accuracy of the digital elevation model (DEM), which itself determines the precision of the canopy model (Dubayah *et al.* 2010). To maximize the accuracy of the DEM, we combined the cloud data of the two acquisitions. Bare-earth points were identified in the global cloud data using the TerraScan (TerraSolid, Helsinki) 'ground' routine, which classifies ground points by iteratively building a triangulated surface model. We manually checked the cloud of points to assess possible issues with this automatic procedure. This led to about 0.35 bare earth points/m^2 over the entire area (out of c.a. 24 imp/m^2 combining the two acquisitions). A DEM grid was subsequently generated at 1-m resolution using the "GridSurfaceCreate" procedure implemented in FUSION v.3.2 (McGaughey 2012). This procedure computes the elevation of each grid cell using the average elevation of all points within the cell (cells containing no bare-earth points are filled by the weighted average of the closest grid points).

Two canopy elevation models were produced with the 2007/8 dataset and with the 2012 dataset. Canopy point outliers were removed automatically by the “FilterData” procedure implemented in FUSION (McGaughey 2012). The canopy model was then constructed at 1-m resolution using the 1-m resolution DEM and the “CanopyModel” procedure implemented in FUSION. This procedure subtracts the elevation model from the return elevation and then uses the highest return value to compute the canopy surface model. The last step consisted in applying a 3x3 neighbour window median filter to smooth the surface and thus avoid local unrealistic maxima or minima. To construct the most recent canopy model, we only considered the last return points (12.5 points/m^2), so as to avoid systematic biases when comparing the two LiDAR datasets. Median canopy height (H_{50}) constructed with LiDAR first returns correlated strongly with that constructed with the last returns (Pearson’s r>0.99), and the mean difference was 0.89 m (median of 0.83).

The 2007/8 LiDAR dataset had a sparser and more heterogeneous coverage and a more heterogeneous point density in space than the 2012 dataset (Fig. S1). To analyse changes in forest structure and carbon stocks, we thus discarded all grid units in which more than 15% of the 1-m^2 pixels contained less than 2 points/m^2 in the 2007/8 dataset (i.e. about half of the mean point density). Exploratory analyses showed that this procedure removed all unrealistic grid values of AGB change while preserving most of the grid units (90.3% of the pixels were kept in the analysis).

2.4. Field data

Seven permanent sampling plots covering a total area of 29.75 ha were established at the Nouragues Ecological Research Station (Fig. 2). In these plots, all living trees ≥ 10 cm of diameter at breast height (DBH) were mapped, censused, and botanically identified by experts during the last decade (67.3% of the 15,438 individuals were identified to at least genus level). DBH was measured at 1.3 m above the ground and to the nearest 0.1 cm. For trees with buttresses, stilt roots or irregularities, trunks were measured 30 cm above the highest irregularity, and the point of measurement was marked with permanent paint. The procedure implemented in the case of a change in the DBH point of measurement between two campaigns is fully described in the supplementary information. One

10-ha plot (called “grand plateau”) and one 12-ha plot (“petit plateau”) were remeasured at the end of 2008, and then again at the end of 2012 (data available from forestplots.net; Lopez-Gonzalez *et al.* 2009, 2011). These two plots are dominated by terra-firme forest, with small flooded forest patches and a ca. 1-ha patch of liana-infested forest (B. Tymen *et al.*, in revision). In 2007, one 6-ha terra-firme forest plot was inventoried ca. 7 km South (“Pararé”, Fig. 2). In 2012, smaller plots were established to encompass the range of forest type variability: one 1-ha plot in an occasionally flooded forest (“Ringler”), two 0.25-ha plots in swamp forest dominated by the palm *Euterpe oleracea*, and one 0.25-ha plot in a low forest on shallow granitic bedrock.

In addition to DBH measurements, we measured the total height of all trees located in plots ≤ 1 ha and in at least one 1-ha subplot in the three larger plots. For a few trees for which accurate measurements were impossible, total height was estimated. In total 2,212 trees had total tree height measured directly. Total tree height was measured by aiming at the tallest branches with a high-resolution laser rangefinder (LaserAce 1000 rangefinder, Trimble, Sunnyvale CA). The built-in inclinometer of this rangefinder has an accuracy of 0.2°, and its distance-measuring device an accuracy of 10 cm at 75 m with a passive target, and a resolution of 1 cm. We targeted the top leaves or branches, moving 180 degrees around the tree in order to locate the highest point, and we also relied on the opinion of at least two trained operators. Total tree height was taken to be the maximum value of several distance measurements. Cross-controls by different operators were regularly conducted to assess the accuracy of our measurements, and these validation checks indicate that our tree height data were on average accurate to the nearest 0.5 m. To infer total tree height for the trees that were not directly measured, we defined plot-specific tree height-diameter allometries of the form:

$$\ln(H) = a + b \times \ln(D) + c \times \ln(D)^2 + \varepsilon \quad (1)$$

where H and D are total tree height and dbh, respectively, and ε is the error term, assumed to be normally distributed with zero mean and residual standard error $\sigma_{\text{log-log model}}$. Model (1) was trained using the tree height ground measurements. The height of all trees was subsequently estimated using Eq (1) and accounting for a known bias by applying the Baskerville correction (see supplementary information; Baskerville 1972):

(2) $$\overline{H} = \exp\left(\sigma_{log-\log model}{}^2/2 + a + b\ln(D) + c\ln(D)^2\right)$$

Model parameters are provided in the supplementary information (Fig. S2 and Table S1).

Ground plots were carefully geo-located by averaging several GPS points at the corners of the plots. We selected one corner and calculated the location of the three other corners using the size and orientation of the plot on the field. A deviation of 18° from the magnetic North Pole to the geographic North Pole was assumed to account for the magnetic singularity over the Guiana Shield. We cross-validated the geolocation using the location of large tree crowns clearly visible in the LiDAR canopy model (Fig. S3).

2.5. Ground AGB *estimation*

In the recent literature, stand-scale AGB was often reported in carbon units and referred to as aboveground carbon density (or ACD). Here we prefer to report values in oven dry biomass units, but it should be borne in mind that 1 kg of dry biomass holds on average 0.48 kg of carbon (Thomas & Martin 2012).Tree aboveground biomass (AGB_t) was estimated using the equation of Chave et al. (2014):

(3) $$AGB_t = 0.0673 \times (\rho \times D^2 \times \overline{H})^{0.976}$$

where ρ is the wood density in g.cm^{-3} and where total height $\overline{H}$ was either measured directly or inferred from equation (2). Wood density ρ was inferred from the taxonomy using a global database (Chave et al. 2009). We assigned a ρ value to each individual tree that corresponded to the mean ρ for species found in the database. We considered only measures that were made in tropical region of South America (n=4,182) in order to limit the bias due to regional variation of wood density (Muller-Landau 2004; Chave et al. 2006). When no reliable species identification or no wood density information at the species level was available, the mean wood density at higher taxonomic level (i.e. genus, family) or at the plot level was assigned to the tree.

The palm *Euterpe oleracea* was dominant in flooded areas. We thus constructed a specific biomass allometry from the destructive harvest data of Miranda et al. (2012) (See supplementary information and Fig. S4 for details and for other error metrics):

(4) $AGB_t = \exp\left(-3.863 + 2.987 \times \ln(D)\right)$ (n=13; $\sigma_{\text{log-log model}}$=0.292)

or

(5) $AGB_t = \exp\left(-3.290 + 0.879 \times \ln(D^2 \times H)\right)$ (n=13; $\sigma_{\text{log-log model}}$=0.205)

AGB was then summed across trees, and normalized by plot area to obtain AGB in Mg ha^{-1}. To estimate AGB in patches of bamboo forest, we conducted a destructive sampling in one 0.125-ha plot of *Guadua sp.* bamboos. In one 10 m x 1 m subplot, we sampled all bamboos ≥ 0.8 cm diameter (36 individuals). The above ground part (stem and leaves) of 13 individuals was oven-dried and weighted, the total dry mass being 4.27 kg. This estimate was then extrapolated to the 0.125-ha plot and the AGB of an isolated tree of *Cecropia obtusa* was added to the estimate using Equation (3).

2.6. Relating LiDAR metrics and stand-scale AGB *estimates*

We carefully coregistered the LiDAR cloud of points and the ground plots by using several GPS datapoints per plot, and also by matching the ground position of emergent trees with the LiDAR canopy model (Fig. S2). LiDAR metrics were calculated within the limits of the calibration plots, ensuring the best spatial match between LiDAR and ground measurements. Stand-scale AGB estimate was fitted against several LiDAR metrics at two different spatial resolutions: 1 ha (100 m x 100 m) and 0.25 ha (50 m x 50 m). To this end, we partitioned our large plots into subplots. We found that median height of the LiDAR canopy model (H_{50}) provided the best fit to ground-based AGB (Table S2). A model selection using H_{50} and any other of these additional LiDAR-based metrics did not provide significantly better model fits than the model including H_{50} alone (Table S3). At both spatial resolutions, we thus fitted independently a log-log linear ordinary least square model of the form:

$$\text{(6)} \qquad \ln(\text{AGB}) = a + b \times \ln\,(H_{50}) + \varepsilon$$

where ε is an error term assumed to be normally distributed with zero mean. After the back-transformation, accounting for the Baskerville correction, stand-scale AGB can thus be inferred from H_{50} using the following model:

$$\text{(7)} \qquad \overline{\text{AGB}} = \exp\left(a + \frac{RSE^2}{2} + b \times \ln\,(H_{50})\right)$$

To facilitate the comparison with previous studies (e.g. Mascaro *et al.* 2011a; Asner *et al.* 2012b; Asner & Mascaro 2014), we also provide equation (7) in the equivalent form:

$$\text{(8)} \qquad \overline{\text{AGB}} = A \times {H_{50}}^{b}$$

where $A = \exp\left(a + \frac{RSE^2}{2}\right)$. Such a power-law model has been shown to predict well AGB from LiDAR metrics (Mascaro et al. 2011a). To fit this statistical model, stand-scale AGB was inferred from the 2012 ground data while H_{50} was calculated from the 2012 LiDAR canopy model, except for the "Pararé" plot where the field data were only available in 2007. In that special case, the 2007/8 LiDAR canopy model was used. We also tested whether AGB model construction based on only the 2007/2008 data or based on only the 2012 data led to different results. We found that the two statistical models relating H_{50} and AGB were very close and thus interchangeable: the mean relative difference across model predictions was within 0.5% of the estimate, and both had the same uncertainty (Fig. S5). We henceforth use only the model based on the 2012 data, thought to be the more accurate.

2.7. LiDAR AGB change

To estimate AGB changes using multiple LiDAR acquisitions, we computed the difference of the two AGB stock layers as derived from the LiDAR metrics and divided the difference by the time elapsed between the two acquisitions, to obtain an annual change in AGB. This procedure was conducted at the 0.25-ha and 1-ha scales. This approach is similar to the "indirect approach" described in Meyer *et al.* (2013) and Skowronski *et al.* (2014), excepted that we used the same LiDAR-AGB model to infer AGB from the two LiDAR datasets (see above; Fig. S5). To validate these products, we compared AGB change as inferred from LiDAR and as measured within the limits of the calibration plots at 0.25 and 1 ha scale using field plots that were surveyed both in 2008 and 2012 (22 ha). The comparison was done with a reduced major axis (RMA) regression that minimizes the sum of squared distances both horizontally (accounting for the error in X) and vertically (accounting for the error in Y) because neither the field-based nor the LiDAR-based AGB changes can be considered as true measurements. Significance was assessed with a test based on the Pearson's product moment correlation coefficient (function "cor.test" in the R statistical software). A second approach would have been to model AGB change directly from change in LiDAR metrics (Skowronski *et al.* 2014). However, because we used the same inversion model for the two datasets, our approach has exactly the same associated error (i.e., the same residual standard error, RSE).

3. Results

3.1. Landscape variation in canopy height

Canopy height, as inferred by LiDAR, revealed a strong spatial structure at the landscape scale (Fig. 2b, Table S4). The maximum registered canopy height was of 67 m and 1% of the 1x1 m pixels had a height > 50 m. A mosaic of low vegetation (<10 m), low forests (10-25 m) and tall forests (>25 m) occurred within the landscape (Fig. 2b and 2c; mean canopy height per vegetation type is given in Table S4). The large patches of low vegetation (2% of the surveyed scene) corresponded predominantly to bamboo thickets or occasionally to Marantaceae or Heliconiaceae patches; low forests correspond to liana forests (1%), flooded forests (13%) or hill-top forests (9%). Tall forests are typical *terra firme* forests (72%).

3.2. Relation between LiDAR metrics and field AGB

Ground-based AGB was significantly predicted by H_{50} both at the 0.25-ha (ratio of the RSE to the prediction mean, RSErel, of 22.3%; $P<0.001$; Fig. 3) and the 1-ha scale (RSErel = 13.8%; $P<0.001$). Alternative models or alternative LiDAR-derived metrics did not display a better statistical performance (table S2). The residuals of this model were not explained by forest type at the 0.25-ha scale (Kruskall-Wallis test, $X^2=2.07$, $P=0.72$), or by variation in wood density across plots (Pearson's $r=0.11$, $P=0.22$) but were spatially autocorrelated (Moran's $I=0.31$, $P<0.001$). The exponent b relating H_{50} to the AGB was close to 1 at the 1-ha scale, thus the relationship was found to be nearly linear. At the 0.25-ha resolution, a few plots were outliers, displaying a much higher ground-based AGB value than inferred using the LiDAR data (Fig. 3). These outlying plots were characterized by a disproportionate number of large-diameter trees.

The AGB map revealed an important spatial structure (Fig. 4a), related to topographical variation (Supplementary information ; Fig. S6). Over the study area, AGB showed a bimodal distribution (Fig. 4b). The first mode corresponded to about 7 % of the total area, and was characteristic of low-vegetation patches, bamboo thickets and of the bare ground of the Inselberg top. The second represented a continuum of closed-canopy forest types. At landscape-scale, mean AGB was estimated to be 344 Mg ha^{-1} (excluding the granitic outcrop). In comparison, mean AGB across plots was 388 Mg ha^{-1}, hence permanent plots tend to be biased towards high-AGB forests (tall forests have a mean landscape AGB of 382 Mg ha^{-1}; Table S4). Mean AGB per forest type within the scene is provided in Table S4.

3.3. Relation between LiDAR metrics and field AGB change

We first compared ground-based AGB change measures and LiDAR-derived ones in the survey plots. We found a significant correlation at 0.25-ha scale, but not at 1-ha scale (Fig. 5). In both cases, the relationship was poor. Across the study area, the LiDAR-derived AGB change map showed that the median change was slightly positive during the study period (median of +0.13 Mg ha^{-1} yr^{-1}), indicating that most patches were accumulating carbon (Fig. 6). However mean AGB change was slightly negative (mean of -0.79 Mg ha^{-1} yr^{-1}). Together, these results suggest that the forest landscape has not increased in AGB during the study period due to some localized large losses of carbon (defined as losses of > 25 Mg ha^{-1} yr^{-1} in localized pixels). The slight negative trend was observed in all forest types with the exception of the granitic outcrop (Table S4). To verify that our results were not influenced by the difference in sensor type from one survey to the next, we constructed independent LiDAR-AGB models using the two LiDAR datasets and showed that they provided undistinguishable predictions (mean relative difference to within 0.5%) with the same associated error (Fig. S5).

4. Discussion

We used two small-footprint LiDAR campaigns to construct a detailed map of canopy structure in an old-growth, high-carbon stock, tropical forest of the Guiana Shield. The landscape was surprisingly heterogeneous, with frequent occurrences of low vegetation patches (liana-infested forests, palm-dominated swamps, bamboo-dominated patches) interspersed within the high-canopy forest matrix. We constructed and validated a statistical model to infer aboveground biomass (AGB) stocks from LiDAR data and we compared the field and LiDAR estimates of AGB changes over a four-year period.

4.1. Inferring AGB *from LiDAR*

Small footprint LiDAR technology was able to detect the fine-grained spatial variation in AGB across a 2,400-ha landscape characterized by both high AGB values (344 Mg ha^{-1} on average in our study area, excluding the granitic outcrop) and a range of tropical forest types. Recently, Taylor et al. (2015) also found that LiDAR was appropriate to map AGB in closed-canopy forests on the Osa Peninsula, Costa Rica, but their mean AGB was much lower than the value reported here (mean of 150-200 Mg ha^{-1} depending on the soil type, see their Figure 3A). In our study, the average AGB stock in permanent plots was 388 Mg ha^{-1}, higher than the landscape-scale average inferred from LiDAR, suggesting that our permanent plots are predominantly established in the dominant high-canopy vegetation type, which has a mean landscape AGB of 382 Mg ha^{-1}. The presence of a mosaic of forest types has a direct bearing on carbon accounting programs. An accurate estimate of carbon storage at the landscape scale critically depends on the representativeness of carbon sampling units. In our study area, topographical elevation was the main driver of forest carbon stocks variation (see also Réjou-Méchain *et al.* (2014) for a global cross-site analysis). Caution should be thus exercised when regional-scale carbon stocks are inferred from permanent sampling plots without assimilating any remote sensing observations or without explicitly taking into account topographical variations (e.g. Malhi *et al.* 2006).

The potential of LiDAR for tropical forest AGB mapping is not novel but most published studies to date have been carried out in tropical forests with AGB typically < 300 Mg/ha (Zolkos *et al.* 2013). The relative error of our LiDAR-AGB model was 13.8% at the 1-ha scale, only slightly higher than previous studies (10-12%; Mascaro et al. 2011a; Meyer et al. 2013), and 22.3% at the 0.25-ha scale. This confirms that small-footprint LiDAR can be used to infer AGB even in high-biomass tropical forests. A common interpretation of the IPCC measuring reporting and verification (MRV) guidelines is that AGB uncertainty should be no more than 20% of the mean (Zolkos *et al.* 2013). Even in our high-biomass forest landscape, the error at 1-ha scale meets these requirements with small footprint LiDAR.

We also attempted to improve the predictive power of this model by exploring its dependence to plot-average wood density or to forest type. The residuals of our models were not explained by either of these factors. However, we found that these residuals were spatially autocorrelated, probably because trees strongly vary in their height-diameter allometric relationships from one area to another one at the landscape scale (Fig. S2). Such spatial autocorrelation in the residuals suggests that the subplots are not independent. Thus the error associated with our LiDAR-AGB model may have been underestimated and using several subplots from a larger field plots is not an optimal strategy from this standpoint.

The performance of our power-law models were similar to that obtained by Mascaro *et al.*

(2011a; b) and Asner *et al.* (2012b, 2013b), lending some credence to the view that universal features in the LiDAR-AGB allometry may exist, in spite of the substantial variation in the power law exponent across forest types (Asner *et al.* 2012). To account for this cross-site variation of model exponents, Asner *et al.* (2012b) and Asner & Mascaro (2014) developed generic models where field data are used to account for cross-site variation in wood density and height-diameter relationships. Asner & Mascaro (2014) found that their model accounted for the variation in the LiDAR-AGB relationship across five contrasted tropical forests (Hawaii, Panama, Madagascar, Colombia and Peru). To further test their generic model, we tested whether it yielded correct results in our study site, and found that it underestimated the stand-scale AGB by 16% (Fig. S7). Because the generic model was originally calibrated with the AGB of trees ≥ 5 cm DBH, and validated in our study with the AGB of trees ≥ 10 cm DBH, the underestimation is probably closer to 20%.Taylor *et al.* (2015) used the approach developed by Asner & Mascaro (2014) but they refitted the parameters of the generic model with their local field data, showing that this model could be applied in other forests but shedding no light on the issue of parameter universality in Asner & Mascaro (2014)'s model. For the sake of completeness, we also conducted the same approach as Taylor *et al.* (2015) at our study site. We found that Asner & Mascaro (2014)'s reparameterized model gave a RMSE of 53.5 $Mg.ha^{-1}$ at the 1-ha scale, higher than with our model reported in Equation 8 (RMSE=52.8 $Mg.ha^{-1}$). The strategy of seeking a universal predictive equation relating LiDAR metrics and AGB is an important step forward, so that Asner and Mascaro (2014)’s model would benefit from including more sites, such as our high-carbon stock forest site. The present study contributes one more study site to this endeavor (raw data are available in Table S5-6).

4.2. Inferring AGB *change from repeated LiDAR acquisitions*

We also compared the ability of repeated LiDAR coverages to detect AGB change due to natural vegetation turnover with ground-based estimate. In our old-growth tropical forest, characterized by a relatively slow dynamics, we showed that LiDAR was able to model, but with very large uncertainties, the fine-scale patterns of variation in AGB change as measured from the ground. Indeed, ground-based AGB change was significantly correlated to LiDAR AGB change at the 0.25-ha scale, but not at the 1-ha scale.

Our study was conducted in a remote forest landscape that is unlikely to have been exposed to significant localized anthropogenic forest disturbances in the past two centuries. Thus, most of the detected changes are likely related to the natural dynamics of the ecosystem. Scaling the estimated LiDAR-AGB change to the study area did not reveal a detectable increase in AGB stock over the study period. Most pixels increased in canopy height (median was positive) but the pixels that lost height had larger losses than the gains. Thus, most forest types were predicted to be a slight source of atmospheric CO_2 during the study period. We emphasize that our LiDAR-AGB change map is highly uncertain, and that given this uncertainty the null hypothesis of no net change cannot be rejected. That said, our result may still be contrasted with a previous study conducted in the same forest but based on tree plots only. Chave *et al.* (2008) found a modest forest carbon sink in the Petit Plateau plot for the period 1992-2000 (+ 0.40 Mg ha^{-1} yr^{-1}), and a larger sink in the Grand Plateau plot (+2.29 Mg ha^{-1} yr^{-1}), and this supported the hypothesis of an increase in AGB in tropical rain forests (Lewis *et al.* 2009). A reanalysis of the same field dataset for the period 2008-2012 gave a very modest sink of + 0.47 Mg ha^{-1} yr^{-1} (Fig. 6), confirming that the area has not significantly increased its AGB stock, as found with the LiDAR-based approach. A similar LiDAR-based approach has been done recently in the Barro Colorado Island (BCI, Panama) where the old growth part of the forest was found to have lost a significant amount of AGB between 1998 and 2009 (Meyer *et al.* 2013). A recent field-based approach confirmed that the old growth forests from BCI have not significantly increased in AGB during the same period (Cushman *et al.* 2014). Together, these observations are in line with the recent findings of Brienen *et al.* (2015), who found a long-term decreasing trend of carbon accumulation in 321 Amazonian field plots.

The AGB changes estimated with repeated LiDAR acquisitions was poorly related to the changes estimated from the field. It suggests that ground-based and LiDAR-based measurements measure different components of forest dynamics and this may be due to several reasons. One interpretation is that natural canopy dynamics is typically dominated by many small-scale events at the top of the canopy, which are associated with branchfalls, rather than treefalls (Kellner & Asner 2009). In our study area, van der Meer and Bongers (1996) previously conducted a careful survey of canopy openings and they found that only a third of natural canopy gaps were larger than 4 m², many such events being caused by branch-falls. A LiDAR sensor will probably pick up these changes in canopy structure but they cannot be detected in ground-based surveys, which generally focus on tree diameter. Such canopy dynamics thus probably contributes to increasing the uncertainty in the comparison between field-based AGB change estimates and LiDAR-based AGB changes (Fig. 5). However, it is unlikely that this effect was the main driver of uncertainties because, contrary to our results, a larger mismatch between field- and LiDAR- AGB change estimates would have been expected at smaller scales, where branch-damage constitute a large fraction of AGB change, than at larger scales. Another source of possible mismatch between the field and LiDAR's field of view is that canopy dynamics, sensed by LiDAR, does not correlate simply with AGB change because woody biomass regenerates more slowly than leaf biomass after a disturbance (Asner *et al.* 2006). Canopy closure following disturbance may also be faster in more disturbed areas (Asner, Keller & Silva 2004), blurring the effect of disturbance on AGB stocks from a canopy field of view. Further, those trees which fall but are alive have lost their canopy position but not their woody biomass, while stand-level wood density can change due to stochastic and deterministic shifts in species composition. Such changes are generally accounted for by ground-based tree-by-tree surveys but not by LiDAR measurements. Finally, even small errors in co-registration between LiDAR maps and ground data or temporal mismatch between the LiDAR and the field campaigns, are likely to weaken the relationship between LiDAR and natural vegetation turnover. In our study, the temporal mismatch between the LiDAR and the field campaigns was of 38% and thus probably increased the mismatch between field- and LiDAR- AGB change estimates.

In natural forests, a major natural cause of AGB change is the large and infrequent gaps formed by multiple tree falls (> 100 m^2 in area). Such rare events are accurately captured by LiDAR at the 0.25-ha resolution but are likely to be averaged out at the 1-ha resolution. In theory, any random change at the pixel scale that is lower than the LIDAR-AGB model RSErel (in our case 13.8% at the 1-ha scale) cannot be detected. However, if changes are concerted across large spatial scales, as is often the case in anthropogenic forest degradation or regrowth, effects of smaller amplitude may be detected (Asner *et al.* 2005). Note also that the eastern and central Amazonia is characterized by a tree turnover that is about half as that measured in southern and western Amazonia (Phillips *et al.* 2004). In western Amazonia, large changes in AGB are thus more frequent than in our study area and we therefore speculate that AGB change may thus be easier to detect by LiDAR in these areas. Finally, in forests exposed to logging activities and/or forest conversion, LiDAR technology is certainly able to map disturbances to a high accuracy (Englhart *et al.* 2013; Andersen *et al.* 2014).

5. Conclusion

Building on the outstanding advances of LiDAR-based technology, we were able to map forest types and estimate AGB stocks of an old-growth tropical forest of French Guiana. Our results show that AGB can be mapped even in a high biomass tropical forest. Given the continuous improvement in LiDAR technology, as well as the decay in the associated operational costs, LiDAR technology will soon provide highly accurate carbon maps over large areas in the tropics (Mascaro *et al.* 2014). This will considerably improve our ability to quantify the carbon stored in the biosphere and thus reduce the uncertainties in the global carbon budget. From an ecological point of view, these fine-scale AGB maps may be used to detect the main ecological controls underpinning forest biomass variability both in space and time. We also showed that the dynamics of old-growth forests is seen differently from a ground or a LiDAR perspective but that the landscape estimate of those two approaches gave consistent conclusions about the overall forest carbon budget. Hence, forest dynamics monitoring would clearly benefit from combining the complementary strengths and insights gained from a top-down and bottom-up views.

Acknowledgments

We acknowledge the hard work of colleagues involved in the 2008-2012 field census campaigns: V. Alt, L. Arnaudet, J. Ateni, C. Baghooa, C. Baraloto, L. Bardon, W. Bétian, V. Bézard, P. Castro, V. Chama Moscoso, P. Châtelet, M. Delaval, A. de la Fuente, J. Engel, M. Fernandez, P. Gaucher, T. Gaui, S. Icho, F. Mazel, M. Noullet, G. Odonne, P. Pétronelli, J. Piton, R. Richnell, A. Sabayo, H. Schimann, J. Tribot, A. Viard-Crétat. We thank R. Pélissier for useful discussions and D. Pflugmacher and three anonymous reviewers for their helpful and constructive comments. We also thank D. Miranda and C. Sanquetta who kindly provided the destructive sampling data of *Euterpe oleracea* and G. Asner and J. Mascaro for useful discussions, and G. Lopez-Gonzalez, J. Ricardo, and G. Pickavance for data and logistical support. We gratefully acknowledge financial support from CNES (postdoctoral grant to MRM, and TOSCA programme), and from "Investissement d'Avenir" grants managed by Agence Nationale de la Recherche (CEBA, ref. ANR-10-LABX-25-01; TULIP: ANR-10-LABX-0041; ANAEE-France: ANR-11-INBS-0001) and the Gordon and Betty Moore Foundation for contributing funding for field recensuses through the RAINFOR project (www.rainfor.org). O.L.P is supported by an ERC Advanced Grant and is a Royal Society-Wolfson Research Merit Award holder. **Contributions**: MRM and JC designed and wrote the paper. MRM and BT analyzed the data and measured tree heights with the help of some abovementioned acknowledged people. All authors contributed to acquiring the field plot inventory data and provided input on draft manuscripts.

References

Agrawal, A., Nepstad, D. & Chhatre, A. (2011) Reducing emissions from deforestation and forest degradation. *Annual Review of Environment and Resources*, **36**, 373–396.

Aldred, A.H. & Bonner, G.M. (1985) Application of airborne laser to forest surveys, Chalk River.

Andersen, H.-E., Reutebuch, S.E., McGaughey, R.J., d' Oliveira, M.V.N. & Keller, M. (2014)

Monitoring selective logging in western Amazonia with repeat lidar flights. *Remote Sensing of Environment*, **151**, 157–165.

Arp, H. & Tranarg, C.A. (1982) Mapping in tropical forests: a new approach using the laser APR [Airborne Profile Recorder]. *Photogrammetric Engineering and Remote Sensing*, **48**.

Asner, G.P., Broadbent, E.N., Oliveira, P.J.C., Keller, M., Knapp, D.E. & Silva, J.N.M. (2006) Condition and fate of logged forests in the Brazilian Amazon. *Proceedings of the National Academy of Sciences*, **103**, 12947–12950.

Asner, G.P., Clark, J.K., Mascaro, J., Vaudry, R., Chadwick, K.D., Vieilledent, G., Rasamoelina, M., Balaji, A., Kennedy-Bowdoin, T., Maatoug, L. & others. (2012a) Human and environmental controls over aboveground carbon storage in Madagascar. *Carbon balance and management*, **7**.

Asner, G.P., Hughes, R.F., Varga, T.A., Knapp, D.E. & Kennedy-Bowdoin, T. (2009) Environmental and biotic controls over aboveground biomass throughout a tropical rain forest. *Ecosystems*, **12**, 261–278.

Asner, G.P., Keller, M. & Silva, J.N. (2004) Spatial and temporal dynamics of forest canopy gaps following selective logging in the eastern Amazon. *Global Change Biology*, **10**, 765–783.

Asner, G.P., Kellner, J.R., Kennedy-Bowdoin, T., Knapp, D.E., Anderson, C. & Martin, R.E. (2013a) Forest canopy gap distributions in the southern peruvian amazon. *PloS one*, **8**, e60875.

Asner, G.P., Knapp, D.E., Broadbent, E.N., Oliveira, P.J.C., Keller, M. & Silva, J.N. (2005) Selective logging in the brazilian Amazon. *Science*, **310**, 480–482.

Asner, G.P. & Mascaro, J. (2014) Mapping tropical forest carbon: Calibrating plot estimates to a simple LiDAR metric. *Remote Sensing of Environment*, **140**, 614–624.

Asner, G.P., Mascaro, J., Anderson, C., Knapp, D.E., Martin, R.E., Kennedy-Bowdoin, T., Breugel, M. van, Davies, S., Hall, J.S., Muller-Landau, H.C., Potvin, C., Sousa, W., Wright, J. & Bermingham, E. (2013b) High-fidelity national carbon mapping for resource management and REDD+. *Carbon Balance and Management*, **8**, 1–14.

Asner, G., Mascaro, J., Muller-Landau, H., Vieilledent, G., Vaudry, R., Rasamoelina, M., Hall, J. & van Breugel, M. (2012b) A universal airborne LiDAR approach for tropical forest carbon mapping. *Oecologia*, **168**, 1147–1160.

Baskerville, G.L. (1972) Use of logarithmic regression in the estimation of plant biomass. *Canadian Journal of Forest Research*, **2**, 49–53.

Bollandsås, O.M., Gregoire, T.G., Næsset, E. & Øyen, B.-H. (2013) Detection of biomass change in a Norwegian mountain forest area using small footprint airborne laser scanner data. *Statistical Methods & Applications*, **22**, 113–129.

Brienen, R.J.W., Phillips, O.L., Feldpausch, T.R., Gloor, E., Baker, T.R., Lloyd, J., Lopez-Gonzalez, G., Monteagudo-Mendoza, A., Malhi, Y., Lewis, S.L. & others. (2015) Long-term decline of the Amazon carbon sink. *Nature*, **519**, 344–348.

Chave, J., Andalo, C., Brown, S., Cairns, M., Chambers, J., Eamus, D., Fölster, H., Fromard, F., Higuchi, N., Kira, T., Lescure, J.-P., Nelson, B., Ogawa, H., Puig, H., Riéra, B. & Yamakura,

T. (2005) Tree allometry and improved estimation of carbon stocks and balance in tropical forests. *Oecologia*, **145**, 87–99.

Chave, J., Coomes, D., Jansen, S., Lewis, S.L., Swenson, N.G. & Zanne, A.E. (2009) Towards a worldwide wood economics spectrum. *Ecology Letters*, **12**, 351–366.

Chave, J., Muller-Landau, H.C., Baker, T.R., Easdale, T.A., Ter Steege, H. & Webb, C.O. (2006) Regional and phylogenetic variation of wood density across 2456 neotropical tree species. *Ecological Applications*, **16**, 2356–2367.

Chave, J., Olivier, J., Bongers, F., Châtelet, P., Forget, P.-M., van der Meer, P., Norden, N., Riéra, B. & Charles-Dominique, P. (2008) Above-ground biomass and productivity in a rain forest of eastern South America. *Journal of Tropical Ecology*, **24**, 355–366.

Chave, J., Réjou-Méchain, M., Búrquez, A., Chidumayo, E., Colgan, M.S., Delitti, W.B.C., Duque, A., Eid, T., Fearnside, P.M., Goodman, R.C., Henry, M., Martínez-Yrízar, A., Mugasha, W.A., Muller-Landau, H.C., Mencuccini, M., Nelson, B.W., Ngomanda, A., Nogueira, E.M., Ortiz-Malavassi, E., Pélissier, R., Ploton, P., Ryan, C.M., Saldarriaga, J.G. & Vieilledent, G. (2014) Improved allometric models to estimate the aboveground biomass of tropical trees. *Global Change Biology*, **20**, 3177–3190.

Clark, D.B. & Kellner, J.R. (2012) Tropical forest biomass estimation and the fallacy of misplaced concreteness. *Journal of Vegetation Science*, **23**, 1191–1196.

Cushman, K.C., Muller-Landau, H.C., Condit, R.S. & Hubbell, S.P. (2014) Improving estimates of biomass change in buttressed trees using tree taper models. *Methods in Ecology and Evolution*, **5**, 573–582.

Drake, J.B., Dubayah, R.O., Clark, D.B., Knox, R.G., Blair, J.B., Hofton, M.A., Chazdon, R.L., Weishampel, J.F. & Prince, S. (2002) Estimation of tropical forest structural characteristics using large-footprint lidar. *Remote Sensing of Environment*, **79**, 305–319.

Drake, J.B., Knox, R.G., Dubayah, R.O., Clark, D.B., Condit, R., Blair, J.B. & Hofton, M. (2003) Above-ground biomass estimation in closed canopy Neotropical forests using lidar remote sensing: factors affecting the generality of relationships. *Global Ecology and Biogeography*, **12**, 147–159.

Dubayah, R.O., Sheldon, S.L., Clark, D.B., Hofton, M.A., Blair, J.B., Hurtt, G.C. & Chazdon, R.L. (2010) Estimation of tropical forest height and biomass dynamics using lidar remote sensing at La Selva, Costa Rica. *Journal of Geophysical Research: Biogeosciences*, **115**, n/a–n/a.

Englhart, S., Jubanski, J. & Siegert, F. (2013) Quantifying dynamics in tropical peat swamp forest biomass with multi-temporal lidar datasets. *Remote Sensing*, **5**, 2368–2388.

Feldpausch, T.R., Banin, L., Phillips, O.L., Baker, T.R., Lewis, S.L., Quesada, C.A., Affum-Baffoe, K., Arets, E.J.M.M., Berry, N.J., Bird, M., Brondizio, E.S., de Camargo, P., Chave, J., Djagbletey, G., Domingues, T.F., Drescher, M., Fearnside, P.M., França, M.B., Fyllas, N.M., Lopez-Gonzalez, G., Hladik, A., Higuchi, N., Hunter, M.O., Iida, Y., Salim, K.A., Kassim, A.R., Keller, M., Kemp, J., King, D.A., Lovett, J.C., Marimon, B.S., Marimon-Junior, B.H., Lenza, E., Marshall, A.R., Metcalfe, D.J., Mitchard, E.T.A., Moran, E.F., Nelson, B.W., Nilus, R., Nogueira, E.M., Palace, M., Patiño, S., Peh, K.S.-H., Raventos, M.T., Reitsma, J.M., Saiz, G., Schrodt, F., Sonké, B., Taedoumg, H.E., Tan, S., White, L., Wöll, H. & Lloyd, J. (2011) Height-diameter allometry of tropical forest trees. *Biogeosciences*, **8**, 1081–

1106.

Feldpausch, T.R., Lloyd, J., Lewis, S.L., Brienen, R.J.W., Gloor, M., Monteagudo Mendoza, A., Lopez-Gonzalez, G., Banin, L., Abu Salim, K., Affum-Baffoe, K., Alexiades, M., Almeida, S., Amaral, I., Andrade, A., Aragão, L.E.O.C., Araujo Murakami, A., Arets, E.J.M.M., Arroyo, L., Aymard C., G.A., Baker, T.R., Bánki, O.S., Berry, N.J., Cardozo, N., Chave, J., Comiskey, J.A., Alvarez, E., de Oliveira, A., Di Fiore, A., Djagbletey, G., Domingues, T.F., Erwin, T.L., Fearnside, P.M., França, M.B., Freitas, M.A., Higuchi, N., E. Honorio C., Iida, Y., Jiménez, E., Kassim, A.R., Killeen, T.J., Laurance, W.F., Lovett, J.C., Malhi, Y., Marimon, B.S., Marimon-Junior, B.H., Lenza, E., Marshall, A.R., Mendoza, C., Metcalfe, D.J., Mitchard, E.T.A., Neill, D.A., Nelson, B.W., Nilus, R., Nogueira, E.M., Parada, A., Peh, K.S.-H., Pena Cruz, A., Peñuela, M.C., Pitman, N.C.A., Prieto, A., Quesada, C.A., Ramírez, F., Ramírez-Angulo, H., Reitsma, J.M., Rudas, A., Saiz, G., Salomão, R.P., Schwarz, M., Silva, N., Silva-Espejo, J.E., Silveira, M., Sonké, B., Stropp, J., Taedoumg, H.E., Tan, S., ter Steege, H., Terborgh, J., Torello-Raventos, M., van der Heijden, G.M.F., Vásquez, R., Vilanova, E., Vos, V.A., White, L., Willcock, S., Woell, H. & Phillips, O.L. (2012) Tree height integrated into pantropical forest biomass estimates. *Biogeosciences*, **9**, 3381–3403.

Harris, N.L., Brown, S., Hagen, S.C., Saatchi, S.S., Petrova, S., Salas, W., Hansen, M.C., Potapov, P.V. & Lotsch, A. (2012) Baseline map of carbon emissions from deforestation in tropical regions. *Science*, **336**, 1573–1576.

Hudak, A.T., Strand, E.K., Vierling, L.A., Byrne, J.C., Eitel, J.U.H., Martinuzzi, S. & Falkowski, M.J. (2012) Quantifying aboveground forest carbon pools and fluxes from repeat LiDAR surveys. *Remote Sensing of Environment*, **123**, 25–40.

Jubanski, J., Ballhorn, U., Kronseder, K., J Franke & Siegert, F. (2013) Detection of large above-ground biomass variability in lowland forest ecosystems by airborne LiDAR. *Biogeosciences*, **10**, 3917–3930.

Kellner, J.R. & Asner, G.P. (2009) Convergent structural responses of tropical forests to diverse disturbance regimes. *Ecology letters*, **12**, 887–897.

Lefsky, M.A., Cohen, W.B., Parker, G.G. & Harding, D.J. (2002) Lidar Remote Sensing for Ecosystem Studies Lidar, an emerging remote sensing technology that directly measures the three-dimensional distribution of plant canopies, can accurately estimate vegetation structural attributes and should be of particular interest to forest, landscape, and global ecologists. *BioScience*, **52**, 19–30.

Lewis, S.L., Lloyd, J., Sitch, S., Mitchard, E.T.A. & Laurance, W.F. (2009) Changing ecology of tropical forests: evidence and drivers. *Annual Review of Ecology, Evolution, and Systematics*, **40**, 529–549.

Lopez-Gonzalez, G., Lewis, S.L., Burkitt, M., Baker, T.R. & Phillips, O.L. (2009) ForestPlots.net Database. *www.forestplots.net. Date of extraction [10,04,2013]*.

Lopez-Gonzalez, G., Lewis, S.L., Burkitt, M. & Phillips, O.L. (2011) ForestPlots. net: a web application and research tool to manage and analyse tropical forest plot data. *Journal of Vegetation Science*, **22**, 610–613.

Malhi, Y., Wood, D., Baker, T.R., Wright, J., Phillips, O.L., Cochrane, T., Meir, P., Chave, J., Almeida, S., Arroyo, L., Higuchi, N., Killeen, T.J., Laurance, S.G., Laurance, W.F., Lewis, S.L., Monteagudo, A., Neill, D.A., Vargas, P.N., Pitman, N.C.A., Quesada, C.A., Salomão, R., Silva, J.N.M., Lezama, A.T., Terborgh, J., Martínez, R.V. & Vinceti, B. (2006) The regional variation of aboveground live biomass in old-growth Amazonian forests. *Global Change Biology*, **12**, 1107–1138.

Mascaro, J., Asner, G.P., Davies, S., Dehgan, A. & Saatchi, S. (2014) These are the days of lasers in the jungle. *Carbon Balance and Management*, **9**, 7.

Mascaro, J., Asner, G.P., Muller-Landau, H.C., Van Breugel, M., Hall, J. & Dahlin, K. (2011a) Controls over aboveground forest carbon density on Barro Colorado Island, Panama. *Biogeosciences*, **8**, 1615–1629.

Mascaro, J., Detto, M., Asner, G.P. & Muller-Landau, H.C. (2011b) Evaluating uncertainty in mapping forest carbon with airborne LiDAR. *Remote Sensing of Environment*, **115**, 3770–3774.

McGaughey, R.J. (2012) FUSION/LDV: Software for LIDAR data analysis and visualization. *US Department of Agriculture, Forest Service, Pacific Northwest Research Station: Seattle, WA, USA*, **123**.

Van der Meer, P.J. & Bongers, F. (1996) Patterns of tree-fall and branch-fall in a tropical rain forest in french guiana. *Journal of Ecology*, **84**, 19–29.

Meyer, V., Saatchi, S.S., Chave, J., Dalling, J.W., Bohlman, S., Fricker, G.A., Robinson, C., Neumann, M. & Hubbell, S. (2013) Detecting tropical forest biomass dynamics from repeated airborne Lidar measurements. *Biogeosciences*, **10**, 5421–5438.

Miranda, D.L.C. de, Sanquetta, C.R., Costa, L.G. da S. & Corte, A.P.D. (2012) Biomassa e carbono em Euterpe oleracea Mart. na ilha do Marajó - PA. *Floresta e Ambiente*, **19**, 336–343.

Muller-Landau, H.C. (2004) Interspecific and inter-site variation in wood specific gravity of tropical trees. *Biotropica*, **36**, 20–32.

Næsset, E., Bollandsås, O.M., Gobakken, T., Gregoire, T.G. & Ståhl, G. (2013) Model-assisted estimation of change in forest biomass over an 11year period in a sample survey supported by airborne LiDAR: A case study with post-stratification to provide "activity data." *Remote Sensing of Environment*, **128**, 299–314.

D' Oliveira, M.V.N., Reutebuch, S.E., McGaughey, R.J. & Andersen, H.-E. (2012) Estimating forest biomass and identifying low-intensity logging areas using airborne scanning lidar in Antimary State Forest, Acre State, Western Brazilian Amazon. *Remote Sensing of Environment*, **124**, 479–491.

Pan, Y., Birdsey, R.A., Fang, J., Houghton, R., Kauppi, P.E., Kurz, W.A., Phillips, O.L., Shvidenko, A., Lewis, S.L. & Canadell, J.G. (2011) A large and persistent carbon sink in the world's forests. *Science*, **333**, 988–993.

Phillips, O.L., Baker, T.R., Arroyo, L., Higuchi, N., Killeen, T.J., Laurance, W.F., Lewis, S.L., Lloyd, J., Malhi, Y., Monteagudo, A., Neill, D.A., Vargas, P.N., Silva, J.N.M., Terborgh, J., Martinez, R.V., Alexiades, M., Almeida, S., Brown, S., Chave, J., Comiskey, J.A., Czimczik, C.I., Di Fiore, A., Erwin, T., Kuebler, C., Laurance, S.G., Nascimento, H.E.M., Olivier, J., Palacios, W., Patino, S., Pitman, N.C.A., Quesada, C.A., Salidas, M., Lezama, A.T. & Vinceti, B. (2004) Pattern and process in Amazon tree turnover, 1976-2001. *Philosophical*

Transactions of the Royal Society of London Series B-Biological Sciences, **359**, 381–407.

Réjou-Méchain, M., Muller-Landau, H.C., Detto, M., Thomas, S.C., Le Toan, T., Saatchi, S.S., Barreto-Silva, J.S., Bourg, N.A., Bunyavejchewin, S., Butt, N., Brockelman, W.Y., Cao, M., Cárdenas, D., Chiang, J.-M., Chuyong, G.B., Clay, K., Condit, R., Dattaraja, H.S., Davies, S.J., Duque, A., Esufali, S., Ewango, C., Fernando, R.H.S., Fletcher, C.D., Gunatilleke, I.A.U.N., Hao, Z., Harms, K.E., Hart, T.B., Hérault, B., Howe, R.W., Hubbell, S.P., Johnson, D.J., Kenfack, D., Larson, A.J., Lin, L., Lin, Y., Lutz, J.A., Makana, J.-R., Malhi, Y., Marthews, T.R., McEwan, R.W., McMahon, S.M., McShea, W.J., Muscarella, R., Nathalang, A., Noor, N.S.M., Nytch, C.J., Oliveira, A.A., Phillips, R.P., Pongpattananurak, N., Punchi-Manage, R., Salim, R., Schurman, J., Sukumar, R., Suresh, H.S., Suwanvecho, U., Thomas, D.W., Thompson, J., Uríarte, M., Valencia, R., Vicentini, A., Wolf, A.T., Yap, S., Yuan, Z., Zartman, C.E., Zimmerman, J.K. & Chave, J. (2014) Local spatial structure of forest biomass and its consequences for remote sensing of carbon stocks. *Biogeosciences*, **11**, 6827–6840.

Saatchi, S.S., Harris, N.L., Brown, S., Lefsky, M., Mitchard, E.T.A., Salas, W., Zutta, B.R., Buermann, W., Lewis, S.L., Hagen, S., Petrova, S., White, L., Silman, M. & Morel, A. (2011) Benchmark map of forest carbon stocks in tropical regions across three continents. *Proceedings of the National Academy of Sciences*, **108**, 9899–9904.

Sabatier, D. & Prévost, M.-F. (1990) Variations du peuplement forestier a l' echelle stationnelle: le cas de la station des Nouragues en Guyane Francaise.

Skowronski, N.S., Clark, K.L., Gallagher, M., Birdsey, R.A. & Hom, J.L. (2014) Airborne laser scanner-assisted estimation of aboveground biomass change in a temperate oak–pine forest. *Remote Sensing of Environment*, **151**, 166–174.

Slik, J.W.F., Paoli, G., McGuire, K., Amaral, I., Barroso, J., Bastian, M., Blanc, L., Bongers, F., Boundja, P., Clark, C., Collins, M., Dauby, G., Ding, Y., Doucet, J.-L., Eler, E., Ferreira, L., Forshed, O., Fredriksson, G., Gillet, J.-F., Harris, D., Leal, M., Laumonier, Y., Malhi, Y., Mansor, A., Martin, E., Miyamoto, K., Araujo-Murakami, A., Nagamasu, H., Nilus, R., Nurtjahya, E., Oliveira, Á., Onrizal, O., Parada-Gutierrez, A., Permana, A., Poorter, L., Poulsen, J., Ramirez-Angulo, H., Reitsma, J., Rovero, F., Rozak, A., Sheil, D., Silva-Espejo, J., Silveira, M., Spironelo, W., ter Steege, H., Stevart, T., Navarro-Aguilar, G.E., Sunderland, T., Suzuki, E., Tang, J., Theilade, I., van der Heijden, G., van Valkenburg, J., Van Do, T., Vilanova, E., Vos, V., Wich, S., Wöll, H., Yoneda, T., Zang, R., Zhang, M.-G. & Zweifel, N. (2013) Large trees drive forest aboveground biomass variation in moist lowland forests across the tropics. *Global Ecology and Biogeography*, n/a–n/a.

Taylor, P., Asner, G., Dahlin, K., Anderson, C., Knapp, D., Martin, R., Mascaro, J., Chazdon, R., Cole, R., Wanek, W., Hofhansl, F., Malavassi, E., Vilchez-Alvarado, B. & Townsend, A. (2015) Landscape-scale controls on aboveground forest carbon stocks on the osa peninsula, costa rica. *PLoS ONE*, **10**, e0126748.

Thomas, S.C. & Martin, A.R. (2012) Carbon Content of Tree Tissues: A Synthesis. *Forests*, **3**, 332–352.

Le Toan, T., Quegan, S., Davidson, M.W.J., Balzter, H., Paillou, P., Papathanassiou, K., Plummer, S., Rocca, F., Saatchi, S., Shugart, H. & Ulander, L. (2011) The BIOMASS mission: Mapping global forest biomass to better understand the terrestrial carbon cycle. *Remote Sensing of Environment*, **115**, 2850–2860.

Vaglio Laurin, G., Chen, Q., Lindsell, J.A., Coomes, D.A., Frate, F.D., Guerriero, L., Pirotti, F. & Valentini, R. (2014) Above ground biomass estimation in an African tropical forest with lidar and hyperspectral data. *ISPRS Journal of Photogrammetry and Remote Sensing*, **89**, 49–58.

Vincent, G., Sabatier, D., Blanc, L., Chave, J., Weissenbacher, E., Pélissier, R., Fonty, E., Molino, J.-F. & Couteron, P. (2012) Accuracy of small footprint airborne LiDAR in its predictions of tropical moist forest stand structure. *Remote Sensing of Environment*, **125**, 23–33.

Zolkos, S.G., Goetz, S.J. & Dubayah, R. (2013) A meta-analysis of terrestrial aboveground biomass estimation using lidar remote sensing. *Remote Sensing of Environment*, **128**, 289–298.

List of Figure Captions

Figure 1: Geographic location of the study area in South America (top right) and in French Guiana (left). The study area of 2,400 ha (bottom right) is illustrated by a hillshade model.

Figure 2: Study area. (a) LiDAR elevation model constructed from combining bare-earth points in the 2007/8 and 2012 LiDAR datasets. A scale bar is given within the panel. **(b)** LiDAR canopy height model (top of canopy height) constructed at a 5-m resolution from the 2012 LiDAR dataset. The dotted lines delineate the 2007/8 LiDAR campaign. (c) Vegetation map obtained by height segmentation of the 2012 canopy model and validated using aerial photography and ground truthing. All areas smaller than 1000 m² were eliminated by removing the longest boundary with an adjacent area (rmarea tool in the v.clean procedure of GRASS). Flooded areas were arbitrarily delimited by a wetness index > 14 and they include both temporary (even rarely) and permanently flooded areas (see Supplementary information).Permanent sampling tree plots are illustrated in red.

Figure 3: Relationship between the aboveground biomass density (AGB) and LiDAR $\boldsymbol{H_{50}}$ for **(a)** 119 plots of 0.25-ha and 1 plot of 0.125 ha (bamboo forest), and (b) 29 plots of 1 ha. The residual standard error (RSE) and the coefficients of the power-law model of equation (8) (see methods) are provided in the bottom-right insets.

Figure 4: Biomass stocks in the Nouragues forests. (a) Map and (b) histogram of the AGB inferred from the 2012 LiDAR-based model at 50-m resolution. The model used to convert LiDAR metrics is displayed in equation (8); for parameters, see figure 4. The landscape mean and standard deviation of AGB were of 339.7 ± 122.2 Mg. ha^{-1}. Similar results were obtained at 100 m resolution (not shown).

Figure 5: Relationship between AGB change estimated from the field and from the LiDAR *H_{50}* including (a) 88 plots of 0.25-ha plots, and (b) 22 plots of 1 ha. The validations were based on 72 0.25-ha plots and 19 1-ha plots, respectively (filled circles). Open circles represent the pixels with less than 2 points/m^2 in the 2007/8 dataset and discarded from the validations (see Methods for the details on data filtering). The slope of a reduced major axis (RMA) regression (solid black line), the residual standard error (RSE), the Pearson's correlation and its corresponding *p* value are provided in insets. The 1:1 line is illustrated by grey dashed lines.

Figure 6: AGB change inferred from the LiDAR model at 50-m resolution. (a) Map over the study area, and (b) histogram of the AGB changes with the mean field based estimates (+ 0.47 Mg ha-1 yr-1; red slashed line). LiDAR AGB change was calculated as the difference between the AGB estimated from the two LiDAR datasets (2012 minus 2007 or 2008). Grid units containing more than 15% of 1-m2 pixels with less than 2 LiDAR points/m^2 in the 2007/8 dataset were discarded. Similar results were obtained at 100 m resolution (not shown).

FIGURES

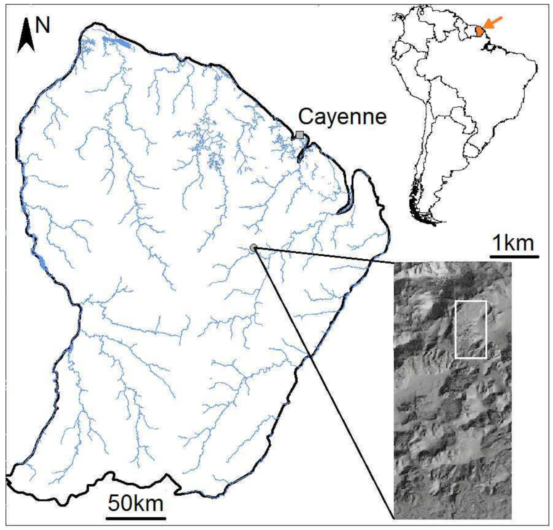

Figure 1: Geographic location of the study area in South America (top right) and in French Guiana (left). The study area of 2,400 ha (bottom right) is illustrated by a hillshade model.

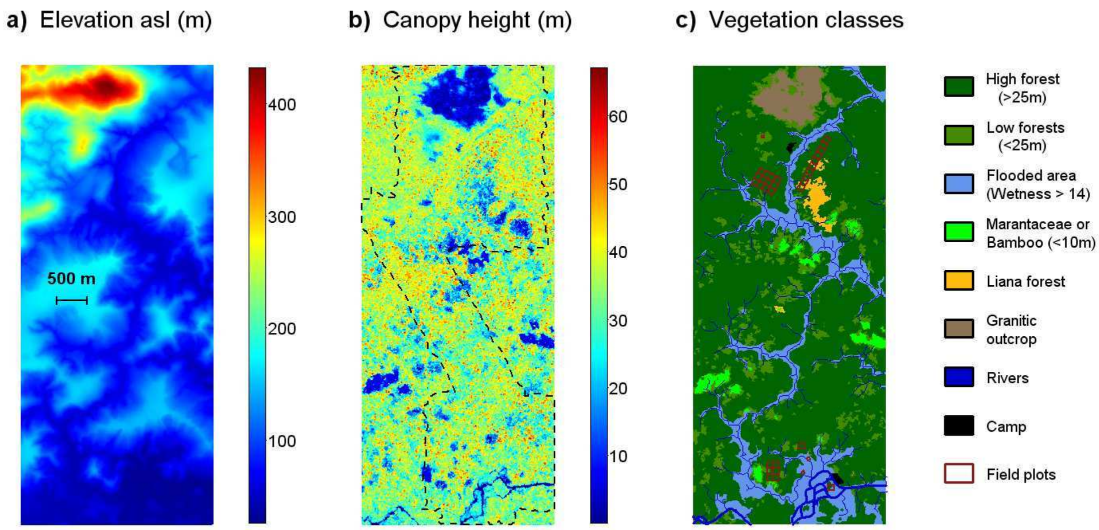

Figure 2: Study area. (a) LiDAR elevation model constructed from combining bare-earth points in the 2007/8 and 2012 LiDAR datasets. A scale bar is given within the panel. **(b)** LiDAR canopy height model (top of canopy height) constructed at a 5-m resolution from the 2012 LiDAR dataset. The dotted lines delineate the 2007/8 LiDAR campaign. (c) Vegetation map obtained by height segmentation of the 2012 canopy model and validated using aerial photography and ground truthing. All areas smaller than 1000 m² were eliminated by removing the longest boundary with an adjacent area (rmarea tool in the v.clean procedure of GRASS). Flooded areas were arbitrarily delimited by a wetness index > 14 and they include both temporary (even rarely) and permanently flooded areas (see Supplementary information).Permanent sampling tree plots are illustrated in red.

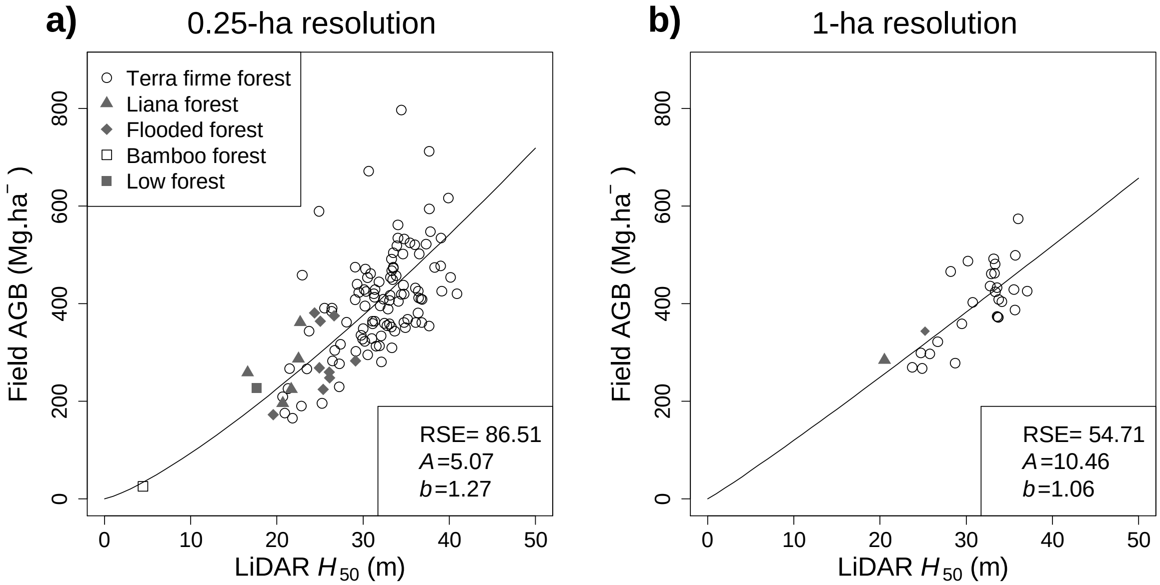

Figure 3: Relationship between the aboveground biomass density (AGB) and LiDAR H_{50} for **(a)** 119 plots of 0.25-ha and 1 plot of 0.125 ha (bamboo forest), and (b) 29 plots of 1 ha. The residual standard error (RSE) and the coefficients of the power-law model of equation (8) (see methods) are provided in the bottom-right insets.

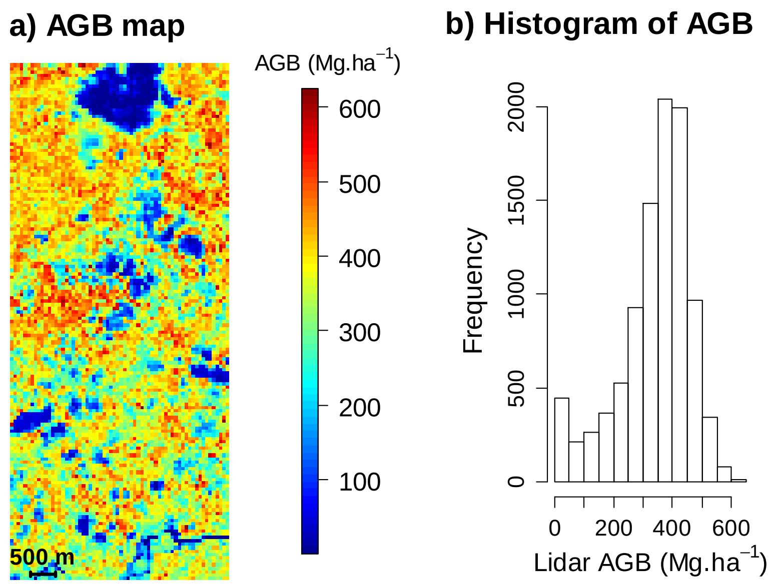

Figure 4: Biomass stocks in the Nouragues forests. (a) Map and (b) histogram of the AGB inferred from the 2012 LiDAR-based model at 50-m resolution. The model used to convert LiDAR metrics is displayed in equation (8); for parameters, see figure 4. The landscape mean and standard deviation of AGB were of 339.7 ± 122.2 Mg. ha^{-1}. Similar results were obtained at 100 m resolution (not shown).

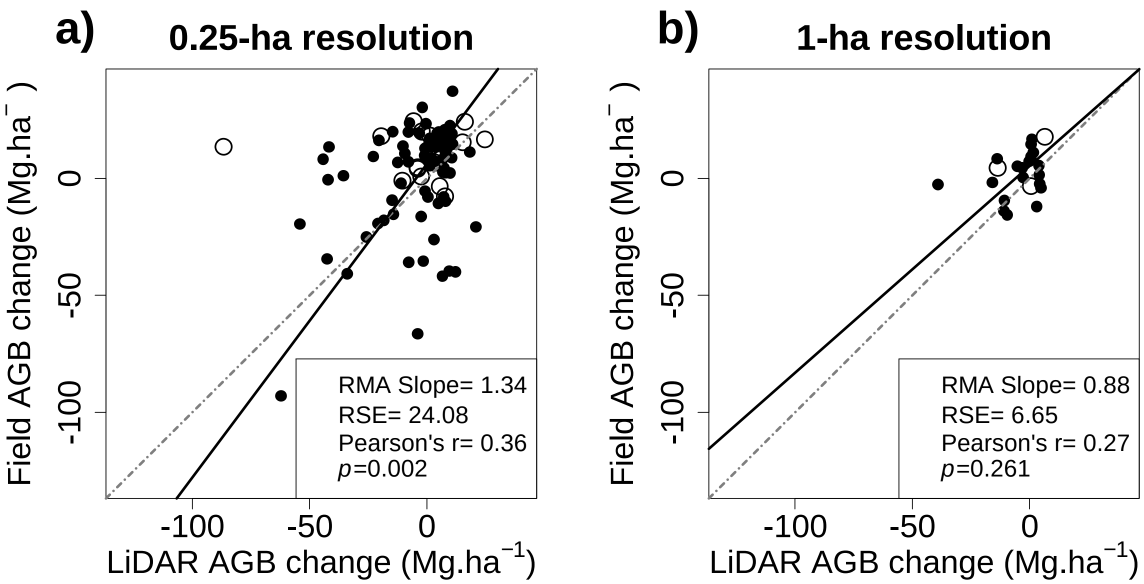

Figure 5: Relationship between AGB change estimated from the field and from the LiDAR $\boldsymbol{H_{50}}$ including (a) 88 plots of 0.25-ha plots, and (b) 22 plots of 1 ha. The validations were based on 72 0.25-ha plots and 19 1-ha plots, respectively (filled circles). Open circles represent the pixels with less than 2 points/m² in the 2007/8 dataset and discarded from the validations (see Methods for the details on data filtering). The slope of a reduced major axis (RMA) regression (solid black line), the residual standard error (RSE), the Pearson's correlation and its corresponding p value are provided in insets. The 1:1 line is illustrated by grey dashed lines.

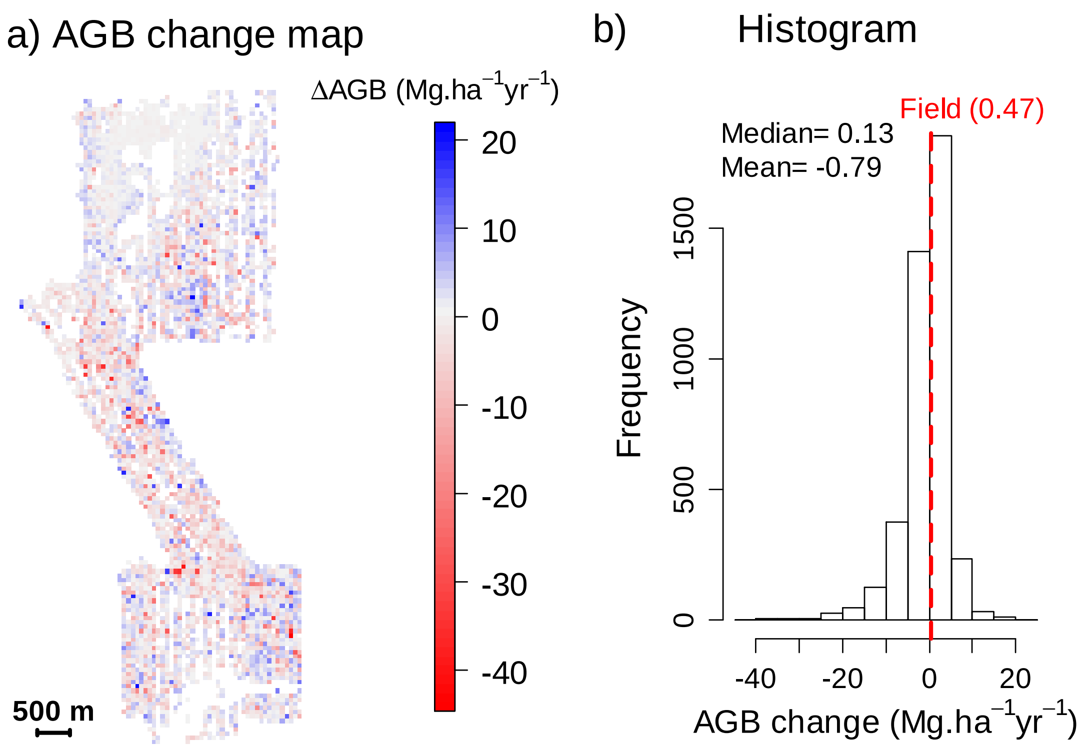

Figure 6: AGB change inferred from the LiDAR model at 50-m resolution. (a) Map over the study area, and (b) histogram of the AGB changes with the mean field based estimates (+ 0.47 Mg ha^{-1} yr^{-1}; red slashed line). LiDAR AGB change was calculated as the difference between the AGB estimated from the two LiDAR datasets (2012 minus 2007 or 2008). Grid units containing more than 15% of 1-m^2 pixels with less than 2 LiDAR points/m² in the 2007/8 dataset were discarded. Similar results were obtained at 100 m resolution (not shown).

Figure 1
Click here to download high resolution image

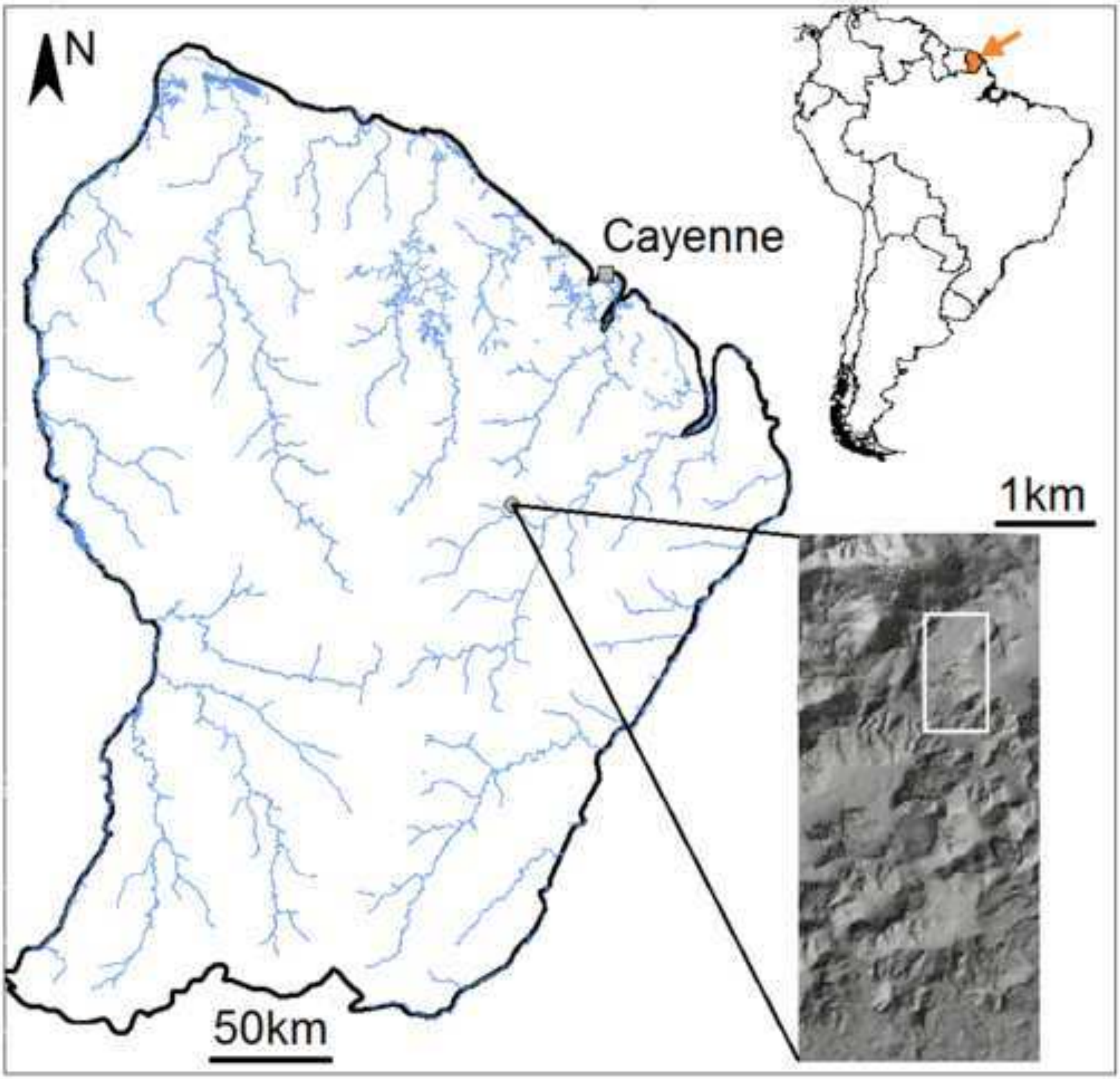

Figure 2

Click here to download Figure: Figure 2.pdf

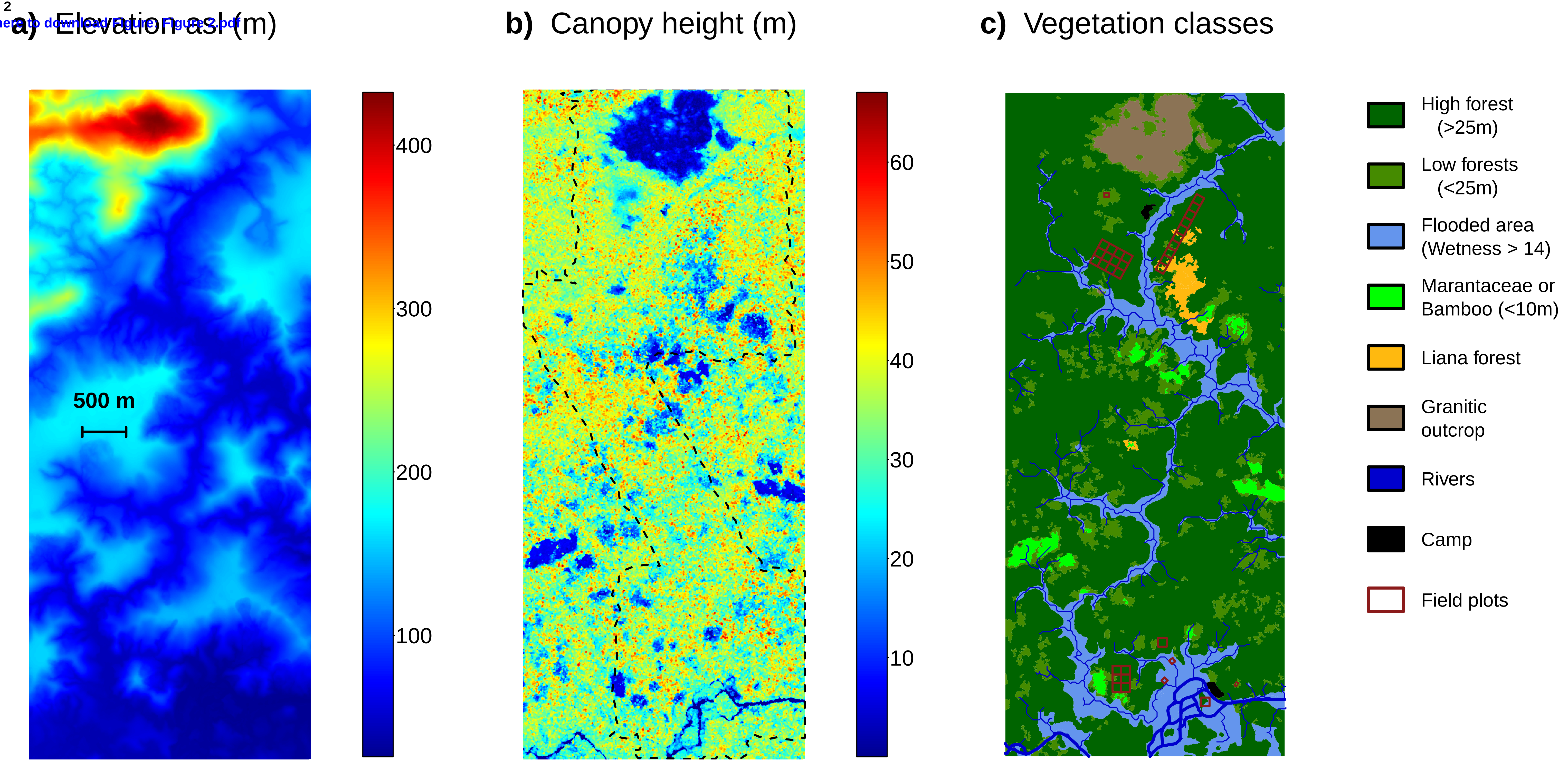

Figure 3
Click here to download Figure: Figure 3.pdf

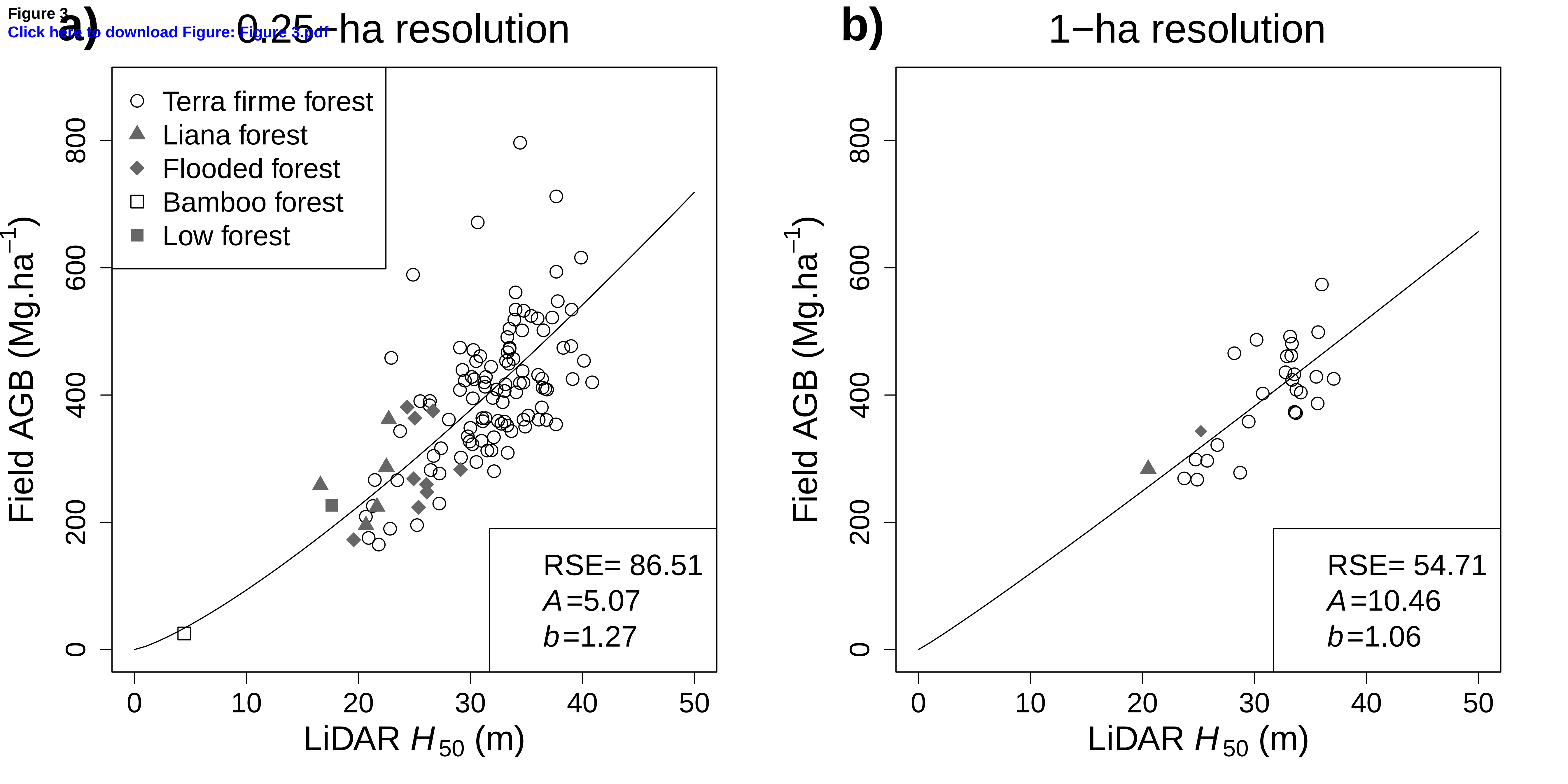

Figure 4

Click here to download Figure: Figure 4.pdf

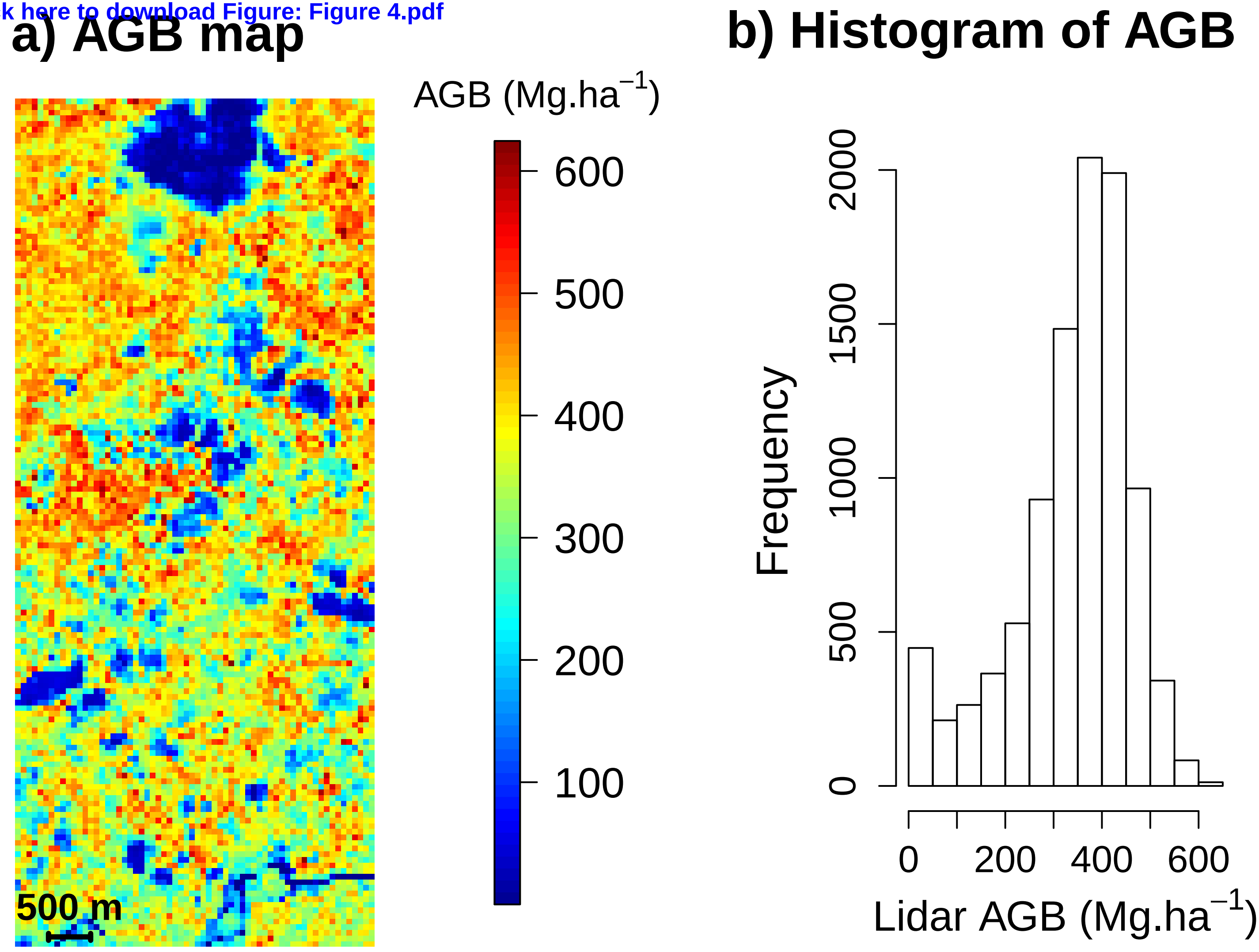

Figure 5
Click here to download Figure: Figure 5.pdf

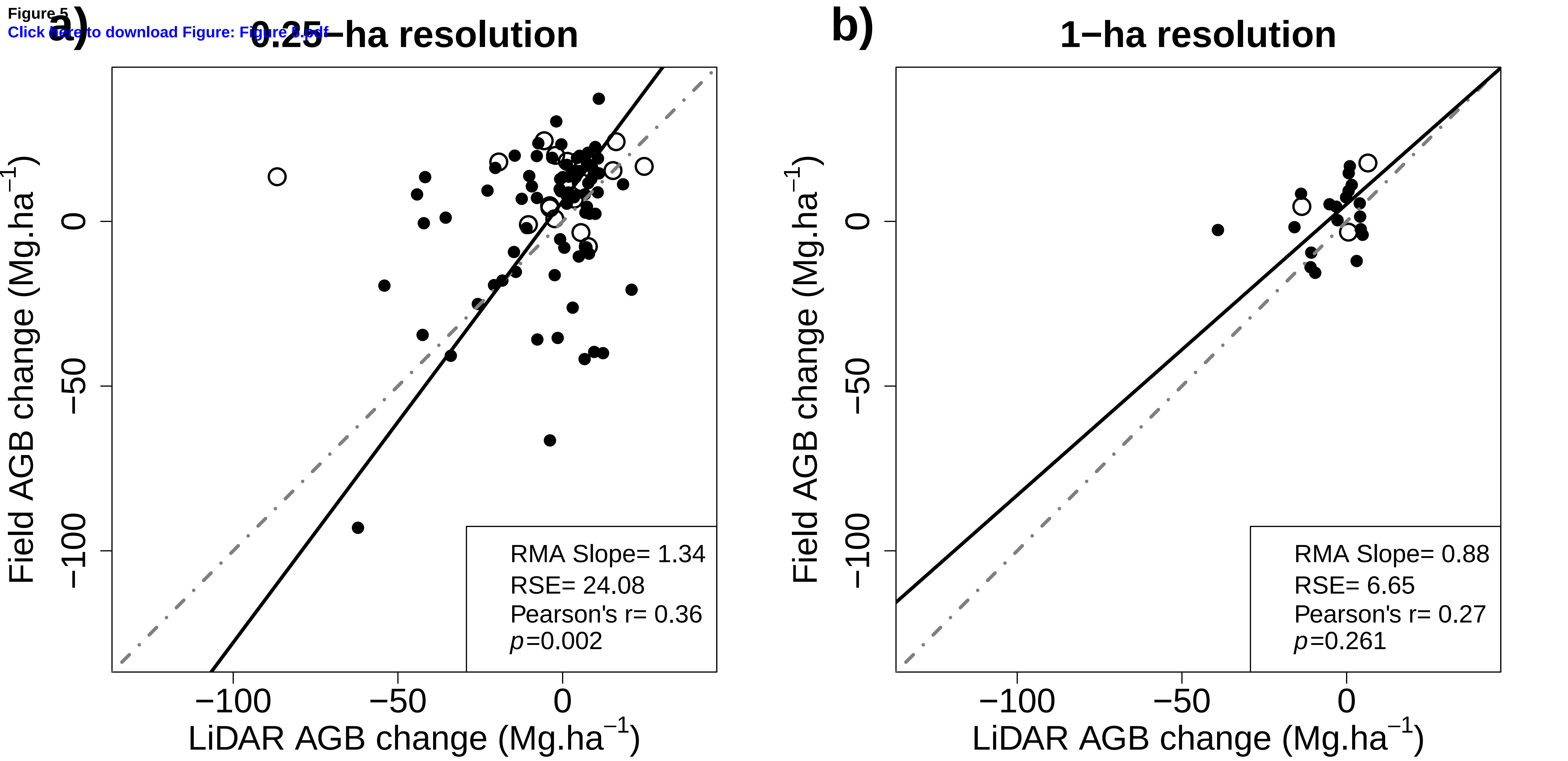

Figure 6

Click here to download Figure: Figure 6.pdf

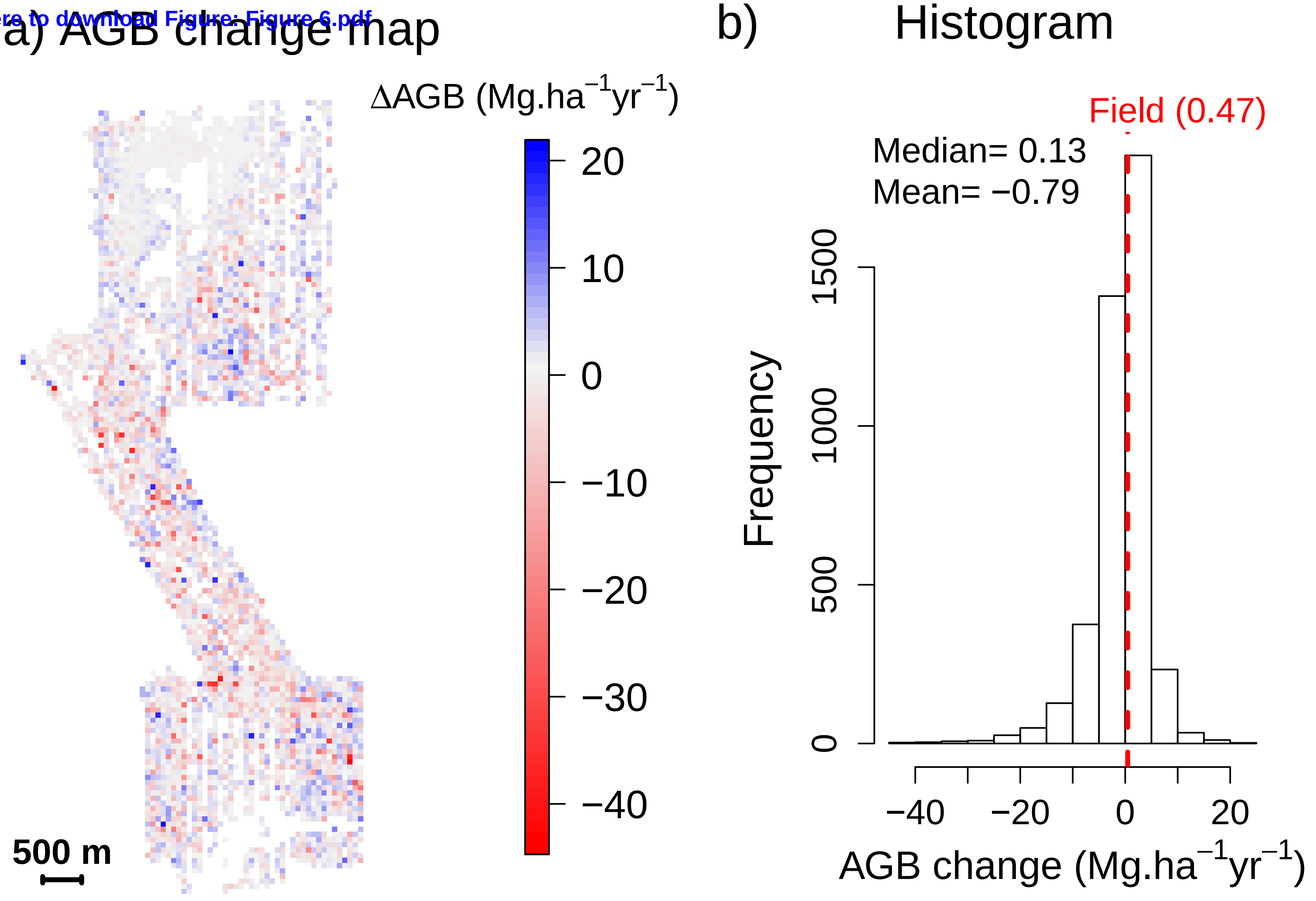

Supplementary Data

Click here to download Supplementary Data: Rejou_LiDAR_AGB_SI_260615.docx